SIAM J. Applied Dynamical Systems
Vol. 15, No. 4, pp. 2051–2077

Stability and Bifurcation in a Stoichiometric Producer-Grazer Model with Knife Edge*

Xianshan Yang†, Xiong Li‡, Hao Wang§, and Yang Kuang¶

Abstract. All organisms are composed of multiple chemical elements such as nitrogen (N), phosphorus (P), and carbon (C). P is essential to build nucleic acids (DNA and RNA) and N is needed for protein production. To keep track of the mismatch between the P requirement in the consumer (grazer) and the P content in the provider (producer), stoichiometric models have been constructed to explicitly incorporate food quality and quantity. In addition to their fundamental applications in ecology and biology, stoichiometric models are especially suitable for medical applications where stoichiometrically distinct pathogens or cancer cells are competing with normal cells and suffer a higher death rate due to excessive chemotherapy agent or radiation uptake. Most stoichiometric models have suggested that the consumer dynamics heavily depends on the P content in the provider when the provider has low nutrient content (low P:C ratio). Motivated by recent lab experiments, researchers explored the effect of excess producer nutrient content (extremely high P:C ratio) on the consumer dynamics. This phenomenon is called the stoichiometric knife edge and its rich dynamics is yet to be appreciated due to the fact that a global analysis of a knife-edge model is challenging. The main challenge stems from the phase plane fragmentation and parameter space partitioning in order to carry out a detailed and complete case by case analysis of the model dynamics. The aim of this paper is to present a sample of a complete mathematical analysis of the dynamics of this model and to perform a bifurcation analysis for the model with Holling type-II functional response.

Key words. stoichiometric knife edge, producer-grazer model, Holling type-II functional response, global stability, equilibria, bifurcation

AMS subject classifications. 34Cxx, 34Dxx, 92D25, 92D40

DOI. 10.1137/15M1023610

1. Introduction.

Well-established mathematical models are effective and powerful to mechanistically explain biological and medical phenomena and to make useful predictions [1, 13, 31]. The historic Lotka–Volterra-type predator-prey models [3, 21, 32] have been of great importance not only in describing cyclic predator-prey dynamics but also in helping policy makers

*Received by the editors May 29, 2015; accepted for publication (in revised form) by E. Kostelich September 7, 2016; published electronically November 1, 2016.
http://www.siam.org/journals/siads/15-4/M102361.html
Funding: The work of the second author was partially supported by the NSFC (11571041) and the Fundamental Research Funds for the Central Universities. The work of the third author was partially supported by the NSERC. The work of the fourth author was partially supported by the NSF grant DMS-1148771 and DMS-1518529.
†School of Information and Mathematics, Yangtze University, Jingzhou, Hubei, 434023, People's Republic of China (24372967@qq.com).
‡School of Mathematical Sciences, Beijing Normal University, Beijing, 100875, People's Republic of China (xli@bnu.edu.cn).
§Corresponding author. Department of Mathematical and Statistical Sciences, University of Alberta, Edmonton, Alberta, T6G 2G1, Canada (hao8@ualberta.ca).
¶School of Mathematical and Statistical Sciences, Arizona State University, Tempe, AZ 85287 (kuang@asu.edu).

propose optimal decisions in natural resource management tasks. However, in many natural systems, human interferences greatly impact the growth rate of populations and dramatically changes their growth environments, often by excessively enriching or limiting some growth limiting resources [9, 10, 26]. For example, the frequent and overuse of fertilizers in farmland leads to eutrophication in nearby lakes and rivers, while the excessive supply of carbon dioxide in greenhouses leads to the lack of micronutrients in plant growth [18, 19, 23]. When an essential nutrient is limiting or in excess in an ecosystem, conventional predator-prey models, which only track the energy flow, cannot adequately describe some of the intriguing and rich ecological observations [11, 20, 27, 28].

To better understand how nutrient availability affects population growth, many stoichiometric population models have been proposed in the past two decades ([15, 33, 34, 35]). One of the well-received stoichiometric producer-grazer models that tracks the quantity and the quality of producer is the one formulated by Loladze, Kuang, and Elser [19]. This model is called the LKE model [30], which describes a food-quality modified Lotka–Volterra-type producer-grazer model. Li, Wang, and Kuang [16] provide a comprehensive review of the rich and complex dynamics of this model. The key assumptions in the LKE model have been relaxed in some follow-up papers such as [33, 34].

Stoichiometric population models are all based on Droop growth equation and the Liebig minimum law governing population growth [2, 17]. These models have found many applications in modeling cancer cell growth and cancer treatments. A malignant tumor often exhibits rapid growth initially due primarily to resource abundance. Gradually, its growth rate tends to decrease as the tumor ages and key resources become limiting [4, 14]. This limitation also provides the impetus for a lasting evolutionary process that enables cancer cells to resist most treatments. In a sequence of two papers, Everett et al. present and compare some cell quota based and clinical date validated treatment models of prostate cancer and chronic myeloid leukemia with some standard population level models in the literature [7, 8]. In addition, Everett et al. also present and systematically study a data validated Droop growth equation based ovarian cancer growth and treatment model with time delay [6]. This simple looking delay population model generates rich dynamics and many novel mathematical questions. As pointed out in [13], there are a few clear advantages of cell quota based population models over other population models. These include (1) the models use well-defined and measurable biological parameters [29]; (2) the models generate good data fit with biologically realistic parameter values [8]; (3) the model parameters are actually functions of the cell quota and hence generate valuable evolutionary insights from the parameter dynamics [24]; (4) the models can be expected to simultaneously fit multiple highly nonlinear or oscillatory data sets depicting several variables observed in the same experimental settings [25].

Recent discoveries in ecological stoichiometry suggest that grazer dynamics are affected by both insufficient and excessive food nutrient content [5]. A typical population growth rate can be viewed as a function of the limiting nutrient. This function can have a single peak and the shape of this function may resemble a knife edge. For this reason, models dealing with excessive nutrient dynamics are called stoichiometric models with knife edge [3, 27]. Elser et al. [3] and Peace et al. [28] modified the LKE model to incorporate the stoichiometric

knife-edge effect:

$$\frac{dx}{dt} = bx\left(1 - \frac{x}{\min\{K, (P-\theta y)/q\}}\right) - \min\left\{f(x), \frac{\hat{f}\theta}{Q}\right\} y, \tag{1.1}$$

$$\frac{dy}{dt} = \min\left\{ef(x), \frac{Q}{\theta}f(x), e\hat{f}\frac{\theta}{Q}\right\} y - dy, \tag{1.2}$$

where

x is the density of producer (mgC/l),
y is the density of grazer (mgC/l),
b is the maximum growth rate of producer (day^{-1}),
K is the producer carrying capacity (mgC/l),
P is the total phosphorus in the system (mgP/l),
q is the minimal P:C in producer (mgP/mgC),
e is the maximal production efficiency of grazer (no unit),
d is the specific loss rate of grazer (day^{-1}),
θ is the grazer's constant P:C (mgP/mgC),
$f(x)$ is the grazer's ingestion rate (day^{-1}), which we take here as a Holling type-II functional response. In general, the function $f(x)$ is a bounded differentiable function that satisfies $f(0) = 0, f'(x) > 0$, and $f''(x) < 0$ for $x \geq 0$ [19]. $f(x)$ satisfies $\lim_{x\to\infty} f(x) = \hat{f}$.

The ratio $Q = \frac{P-\theta y}{x}$ describes the variable phosphorus quota of the producer.

Peace et al. [28] provided a basic analysis and obtained some criteria to determine the local stability of equilibria and presented numerical simulations to illustrate the rich dynamics of their stoichiometric knife-edge model. In this paper, we provide a rigorous mathematical analysis for local and global stability results of all equilibria and the existence of limit cycles. We also provide a rigorous bifurcation analysis, with respect to the total phosphorus parameter P (representing the nutrient status in the system), for the model with Holling type-II functional response. The rigorous analysis of this nonsmooth model is mathematically challenging due to its three minimum functions.

2. Basic analysis. In this section, we present a basic analysis of the model (1.1)–(1.2). We will establish the boundedness of solutions and the local stability of equilibria on the boundary. The basic assumptions for the model are the following:

(i) $f(x) = \frac{cx}{a+x}$ (Holling type-II functional response). Here the parameter c is the maximal ingestion rate of the grazer (day^{-1}), and a represents the half-saturation of the grazer ingestion response (mgC/l). Hence $\hat{f} = c$;
(ii) $e < 1$ (due to the thermodynamic limitations);
(iii) $q/\theta < e$ (since θ is usually much larger than q).

For simplicity, we scale the system by

$$P/\theta \to P, \quad q/\theta \to q, \quad b/c \to b, \quad d/c \to d, \quad cdt \to dt,$$

to obtain the new system

$$\frac{dx}{dt} = bx\left(1 - \frac{x}{\min\{K,(P-y)/q\}}\right) - \min\left\{\frac{1}{a+x}, \frac{1}{P-y}\right\} xy$$

$$\triangleq xF(x,y), \tag{2.1}$$

$$\frac{dy}{dt} = \min\left\{\frac{ex}{a+x}, \frac{P-y}{a+x}, \frac{ex}{P-y}\right\} y - dy \triangleq yG(x,y). \tag{2.2}$$

Here

$$F(x,y) = b\left(1 - \frac{x}{\min\{K,(P-y)/q\}}\right) - \min\left\{\frac{1}{a+x}, \frac{1}{P-y}\right\} y$$

$$= \begin{cases} b\left(1-\frac{x}{K}\right) - \frac{y}{a+x}, & x+y \geq P-a, y \leq P-qK, \\ b\left(1-\frac{x}{K}\right) - \frac{y}{P-y}, & x+y < P-a, y \leq P-qK, \\ b\left(1-\frac{qx}{P-y}\right) - \frac{y}{a+x}, & x+y \geq P-a, y > P-qK, \\ b\left(1-\frac{qx}{P-y}\right) - \frac{y}{P-y}, & x+y < P-a, y > P-qK. \end{cases}$$

$$G(x,y) = \min\left\{\frac{ex}{a+x}, \frac{P-y}{a+x}, \frac{ex}{P-y}\right\} - d$$

$$= \begin{cases} \frac{ex}{a+x} - d, & ex+y \leq P, x+y \geq P-a, \\ \frac{P-y}{a+x} - d, & ex+y > P, ex(a+x) > (P-y)^2, \\ \frac{ex}{P-y} - d, & x+y < P-a, ex(a+x) < (P-y)^2. \end{cases}$$

Let

$$k = \begin{cases} K, & P \geq qK, \\ P/q, & P < qK, \end{cases}$$

$$\Omega = \{(x,y) : 0 < x < k, 0 < y < P, qx + y < P\}.$$

If $k = K$, then Ω is an open trapezoid (see Figure 1(a)). If $k = P/q$, then Ω is an open triangle (see Figure 1(b)).

2.1. Boundedness of solutions. The set Ω represents initial points that make biological sense due to the conservation and limitation of nutrient. We show below that if the initial point $(x(0), y(0))$ lies in Ω, then the solution stays in it. See Appendix A for the proof.

Theorem 2.1 (dissipativity). *Ω is positively invariant for the semiflow generated by system (2.1)–(2.2).*

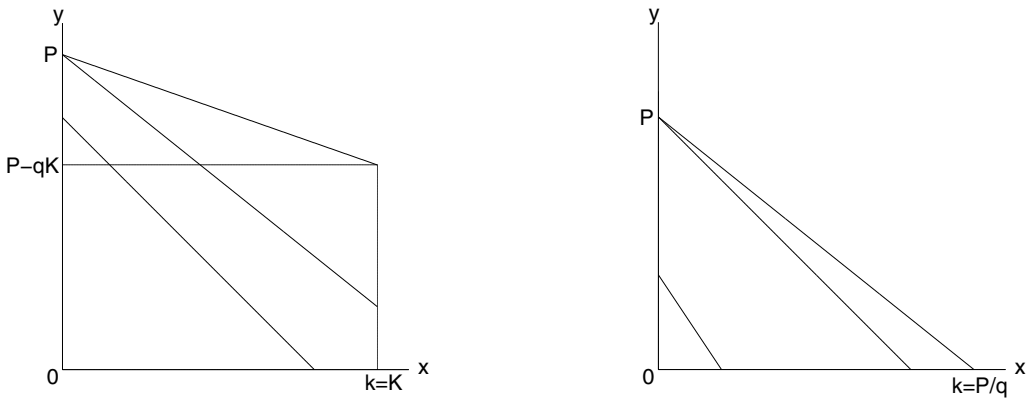

(a) The phase space Ω for $k = K$.

(b) The phase space Ω for $k = P/q$.

Figure 1. *The phase space Ω. When $k = K$, Ω is an open trapezoid, while when $k = P/q$, Ω ia an open triangle.*

2.2. Boundary equilibria. In this subsection, we examine the stability of equilibria on the boundary. It is easy to see that the boundary equilibria of system (2.1)–(2.2) are $E_0 = (0, 0)$ and $E_1 = (k, 0)$.

We can show the following theorem for the stability of the boundary equilibria. The proof is presented in Appendix B. The mathematical challenge is the nonsmoothness of the model due to minimum functions.

Theorem 2.2 (boundary stability). *For system (2.1)–(2.2), the origin E_0 is an unstable saddle, and the only direction towards E_0 is y-axis. For the equilibrium E_1, it is a locally asymptotically stable (LAS) node if one of the following cases is true:*

(1) $q < d, P < qK$;
(2) $P < \min\{qK, adq/(q - d)\}$;
(3) $eK < d(a + K)$, $eK < P < a + K$;
(4) $qK < P < \min\{d(a + K), eK\}$;
(5) $P > \max\{qK, a + K, eK/d\}$.

Otherwise, E_1 is an unstable saddle.

3. Global analysis of the model. In this section, we investigate the stability of equilibria and perform a bifurcation analysis of the system (2.1)–(2.2). Since the model has nine parameters, it is a daunting task to carry out a complete analysis of the system. We instead provide a glimpse of the rich dynamics embodied by system (2.1)–(2.2) by presenting a sample analysis with all parameters fixed except the total phosphorus P. Our bifurcation analysis provides a rigorous mathematical proof for the numerical bifurcation diagram of the total phosphorus. This is mathematically challenging due to the complicated structure of the nonsmooth model.

We fix all parameters except P with the following realistic values: $b = 1.2$ (/day), $K = 1.5$ (mgC/l), $q = 0.0038$ (mgP/mgC), $e = 0.8$, $d = 0.25$ (/day), $\theta = 0.03$ (mgP/mgC), $c = 0.81$ (/day), $a = 0.25$ (mgC/l). These values were used by Loladze, Kuang, and Elser [19] and Peace, Wang, and Kuang [27]. The parameter P has the range: 0-0.2 (mgP/l). With the

above parameter values, we have

$$
\begin{aligned}
f(x) = \frac{cx}{a+x} &= \frac{81x}{25+100x}, \hat{f} = c = 0.81,\\
\min\left\{K, \frac{P-\theta y}{q}\right\} &= \min\left\{\frac{3}{2}, \frac{5000}{19}P - \frac{150}{19}y\right\},\\
\min\left\{f(x), \frac{\hat{f}\theta x}{P-\theta y}\right\} &= \min\left\{\frac{81x}{25+100x}, \frac{81x}{\frac{10000}{3}P-100y}\right\},\\
\min\left\{ef(x), \frac{P-\theta y}{\theta x}f(x), e\hat{f}\frac{\theta x}{P-\theta y}\right\}&\\
&= \min\left\{\frac{324x}{125+500x}, \frac{2700P-81y}{25+100x}, \frac{324x}{\frac{50000}{3}P-500y}\right\}.
\end{aligned}
$$

The model becomes

$$
\begin{aligned}
\frac{dx}{dt} &= \frac{6}{5}x\left(1 - \frac{x}{\min\{\frac{3}{2}, \frac{5000}{19}P - \frac{150}{19}y\}}\right)\\
&\quad - \min\left\{\frac{81x}{25+100x}, \frac{81x}{\frac{10000}{3}P-100y}\right\}y, \qquad (3.1)\\
\frac{dy}{dt} &= \min\left\{\frac{324x}{125+500x}, \frac{2700P-81y}{25+100x}, \frac{324x}{\frac{50000}{3}P-500y}\right\}y - \frac{1}{4}y. \qquad (3.2)
\end{aligned}
$$

The phase space $\Omega = \{(x,y) : 0 < x < \frac{3}{2}, 0 < y < \frac{100}{3}P, 19x + 150y < 5000P\}$. When $P \geq 0.0057$, Ω is an open trapezoid, while for $P < 0.0057$, Ω is an open triangle. From Theorem 2.1, one can obtain the following result.

Corollary 3.1. *Ω is a positively invariant set for the flow generated by system (3.1)–(3.2).*

To simplify the analysis, we rewrite system (3.1)–(3.2) in the following form:

$$
\begin{aligned}
\frac{dx}{dt} &= xF(x,y),\\
\frac{dy}{dt} &= yG(x,y),
\end{aligned}
$$

where

$$
\begin{aligned}
F(x,y) &= \frac{6}{5} - \frac{6x/5}{\min\{\frac{3}{2}, \frac{5000}{19}P - \frac{150}{19}y\}} - \min\left\{\frac{81}{25+100x}, \frac{81}{\frac{10000}{3}P-100y}\right\}y\\
&= \begin{cases}
\frac{6}{5} - \frac{4}{5}x - \frac{81y}{25+100x}, & y \leq \frac{100}{3}P - 0.19, x + y \geq \frac{100}{3}P - \frac{1}{4},\\
\frac{6}{5} - \frac{4}{5}x - \frac{81y}{\frac{10000}{3}P-100y}, & x + y < \frac{100}{3}P - \frac{1}{4},\\
\frac{6}{5} - \frac{57x}{12500P-375y} - \frac{81y}{25+100x}, & y > \frac{100}{3}P - 0.19,
\end{cases}
\end{aligned}
$$

and

$$G(x,y)=\min\left\{\frac{324x}{125+500x},\frac{2700P-81y}{25+100x},\frac{324x}{\frac{50000}{3}P-500y}\right\}-\frac{1}{4}$$
$$=\begin{cases}\frac{324x}{125+500x}-\frac{1}{4}, & 0.8x+y\le\frac{100}{3}P, x+y\ge\frac{100}{3}P-\frac{1}{4},\\ \frac{2700P-81y}{25+100x}-\frac{1}{4}, & 0.8x+y>\frac{100}{3}P,\\ \frac{324x}{\frac{50000}{3}P-500y}-\frac{1}{4}, & x+y<\frac{100}{3}P-\frac{1}{4}.\end{cases}$$

The partial derivatives of F and G exist almost everywhere on Ω:

$$F_x=\begin{cases}-\frac{4}{5}+\frac{324y}{(5+20x)^2}, & y<\frac{100}{3}P-0.19, x+y>\frac{100}{3}P-\frac{1}{4},\\ -\frac{4}{5}, & x+y<\frac{100}{3}P-\frac{1}{4},\\ -\frac{57}{12500P-375y}+\frac{324y}{(5+20x)^2}, & y>\frac{100}{3}P-0.19;\end{cases}$$
$$F_y=\begin{cases}-\frac{81}{25+100x}, & y<\frac{100}{3}P-0.19, x+y>\frac{100}{3}P-\frac{1}{4},\\ -\frac{27P}{(\frac{100}{3}P-y)^2}, & x+y<\frac{100}{3}P-\frac{1}{4},\\ -\frac{855x}{(2500P-75y)^2}-\frac{81}{25+100x}, & y>\frac{100}{3}P-0.19;\end{cases}$$
$$G_x=\begin{cases}\frac{1620}{(25+100x)^2}, & 0.8x+y<\frac{100}{3}P, x+y>\frac{100}{3}P-\frac{1}{4},\\ -\frac{10800P-324y}{(5+20x)^2}, & 0.8x+y>\frac{100}{3}P,\\ \frac{81}{\frac{12500}{3}P-125y}, & x+y<\frac{100}{3}P-\frac{1}{4};\end{cases}$$
$$G_y=\begin{cases}0, & 0.8x+y<\frac{100}{3}P, x+y>\frac{100}{3}P-\frac{1}{4},\\ -\frac{81}{25+100x}, & 0.8x+y>\frac{100}{3}P,\\ \frac{1620x}{(\frac{5000}{3}P-50y)^2}, & x+y<\frac{100}{3}P-\frac{1}{4}.\end{cases}$$

3.1. Nullclines. The x-nullcline is $x=0$ and $F(x,y)=0$. If $y<\frac{100}{3}P-0.19$ and $x+y<\frac{100}{3}P-\frac{1}{4}$, $F(x,y)=0$ determines a hyperbola

$$xy-\frac{100}{3}Px-\frac{201}{80}y+50P=0.$$

In order to investigate whether this hyperbola will or will not enter the domain $\{(x,y)\in\Omega: x+y>\frac{100}{3}P-\frac{1}{4}\}$, we need to know the relative position relationship among these curves $xy-\frac{100}{3}Px-\frac{201}{80}y+50P=0$ (denote by Γ_1) and $x+y=\frac{100}{3}P-\frac{1}{4}$ (denote by l_1). If the hyperbola Γ_1 and the line l_1 intersect, denote these intersections as A_1 (left) and A_2 (right); the coordinates of A_1 and A_2 are determined by the equations

$$xy-\frac{100}{3}Px-\frac{201}{80}y+50P=0,$$
$$x+y=\frac{100}{3}P-\frac{1}{4},$$

i.e., their coordinates are

$$x_{A_1} = \frac{1}{160}\left[181 - \sqrt{48841 - 864000P}\right], \quad y_{A_1} = \frac{100}{3}P - \frac{1}{4} - x_{A_1},$$
$$x_{A_2} = \frac{1}{160}\left[181 + \sqrt{48841 - 864000P}\right], \quad y_{A_2} = \frac{100}{3}P - \frac{1}{4} - x_{A_2}.$$

Denote by A the hyperbola Γ_1 and y-axis, i.e., the y-coordinate of A is

$$y_A = \frac{4000}{201}P.$$

By simple calculation, we can obtain the following result.

If $P > 0.056529$, then the hyperbola Γ_1 and the line l_1 do not intersect, which implies that the hyperbola Γ_1 will not enter the domain $\{(x, y) \in \Omega : x + y > \frac{100}{3}P - \frac{1}{4}\}$. In other words, the x-nullcline $F(x, y) = 0$ determines a hyperbola Γ_1.

If $0.018611 < P < 0.056529$, then $0 < x_{A_1} < 1.13016$, which implies that the hyperbola Γ_1 will enter the domain $\{(x, y) \in \Omega : x+y > \frac{100}{3}P-\frac{1}{4}\}$. We also note that when $y < \frac{100}{3}P-0.19$ and $x + y > \frac{100}{3}P - \frac{1}{4}$, $F(x, y) = 0$ determines a parabola

$$y = \frac{10}{81}(3 - 2x)(1 + 4x) \triangleq g(x).$$

The maximum of $g(x)$ is

$$y_{\max} = g\left(\frac{5}{8}\right) \approx 0.756173.$$

If $P < 0.028385$, then $\frac{100}{3}P - 0.19 < 0.756173$, which implies that the parabola $y = g(x)$ will enter the domain $\{(x, y) \in \Omega : y > \frac{100}{3}P - 0.19\}$. Therefore, when $0.018611 < P < 0.028385$, the x-nullcline $F(x, y) = 0$ is joint with three parts, a hyperbola Γ_1, a parabola $y = g(x)$, and another hyperbola $\frac{19x}{5000P-150y} + \frac{27y}{10+40x} = 1$ (denote by Γ_2). When $0.028385 < P < 0.056529$, the x-nullcline $F(x, y) = 0$ is joint with two parts, one is the hyperbola Γ_1, the other is the parabola $y = g(x)$.

If $0.0057 < P < 0.018611$, then $x_{A_1} < 0$ and $x_{A_2} > 2.2625 > 1.5$, which implies that the hyperbola Γ_1 lies out of the domain $\{(x, y) \in \Omega : x + y < \frac{100}{3}P - \frac{1}{4}\}$; in other words, the x-nullcline $F(x, y) = 0$ is joint with two parts, one is the parabola $y = g(x)$, the other is a hyperbola Γ_2.

If $P < 0.0057$, then $\frac{100}{3}P - 0.19 < 0$, the phase space Ω becomes an open triangle, the x-nullcline $F(x, y) = 0$ determines a hyperbola Γ_2.

The y-nullcline is simpler, which is the x-axis and a piecewise linear segment

$$x = \frac{125}{796} \approx 0.157035, \quad \frac{100}{3}P - \frac{1}{4} - x < y < \frac{100}{3}P - 0.8x,$$
$$x + 3.24y = 108P - 0.25, \quad 0.8x + y > \frac{100}{3},$$
$$2.592x + y = \frac{100}{3}P, \quad x + y < \frac{100}{3}P - \frac{1}{4},$$

determined by $G(x, y) = 0$ (see Figures 2–7).

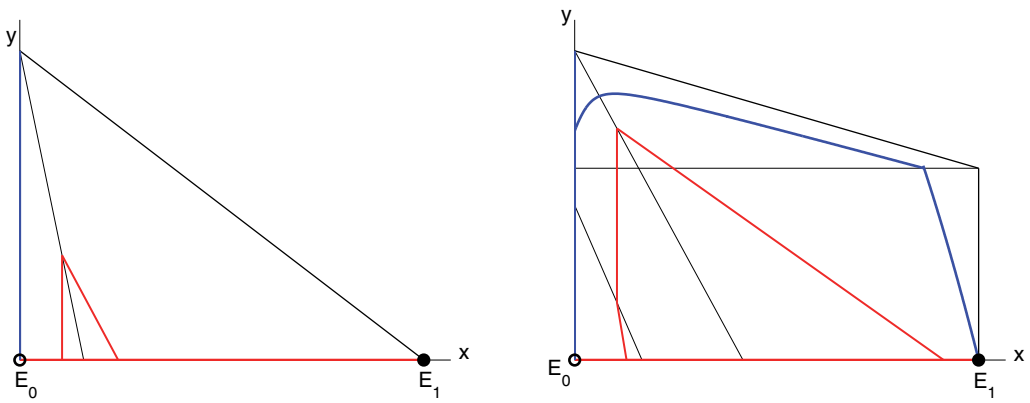

(a) $P < 0.0057$. (b) $0.0057 < P < 0.016204$.

Figure 2. *The nullclines and equilibria for $P < 0.016204$. There exist no internal equilibria.*

3.2. Equilibria and their stabilities. The system (3.1)–(3.2) has two boundary equilibria $E_0 = (0, 0)$ and $E_1 = (k, 0)$, where $k = \frac{5000}{19}P$ if $P < 0.0057$, and $k = 1.5$ if $P \geq 0.0057$. According to Theorem 2.2, we obtain the following result about the stability of boundary equilibria.

Corollary 3.2. *The system (3.1)–(3.2) has two boundary equilibria E_0 and E_1. The origin E_0 is an unstable saddle, and the only direction towards E_0 is the y-axis. For the stability of the equilibrium E_1, there are three cases:*

If $0.016204 < P < 0.116640$, the equilibrium E_1 is an unstable saddle;
If $P < 0.016204$ or $P > 0.116640$, the equilibrium E_1 is an LAS node;
If $P = 0.016204$ or $P = 0.116640$, the equilibrium E_1 is a saddle node.

Now we start to analyze the system (3.1)–(3.2) according to the parameter P.

- Case 1. $0 < P \leq 0.016204$.
- Case 2. $0.016204 < P < 0.028408$.
- Case 3. $0.028408 \leq P \leq 0.031510$.
- Case 4. $0.031510 < P < 0.116640$.
- Case 5. $0.116640 \leq P \leq 0.121203$.
- Case 6. $0.121203 < P \leq 0.2$.

3.2.1. Case 1. $0 < P \leq 0.016204$. The system has only the boundary equilibria $E_0 = (0, 0), E_1 = (k, 0)$, and no internal equilibria exist in this case. If $0 < P < 0.0057$, then $P/q < K = 1.5$, thus the phase space Ω is an open triangle and $k = P/q$ (see Figure 2(a)). If $0.0057 \leq P < 0.016204$, then the phase space Ω is an open trapezoid, $k = 1.5$ (see Figure 2(b)). E_0 is a saddle, E_1 is a globally asymptotically stable (GAS) node. If $P = 0.016204$, E_1 is a saddle node and a transcritical bifurcation appears. All orbits in Ω tend to E_1 in this case, which implies that the grazer cannot survive due to starvation.

3.2.2. Case 2: $0.016204 < P < 0.028408$. In this case, the system has internal equilibria. In order to investigate the locations of them and discuss their stability, we need to

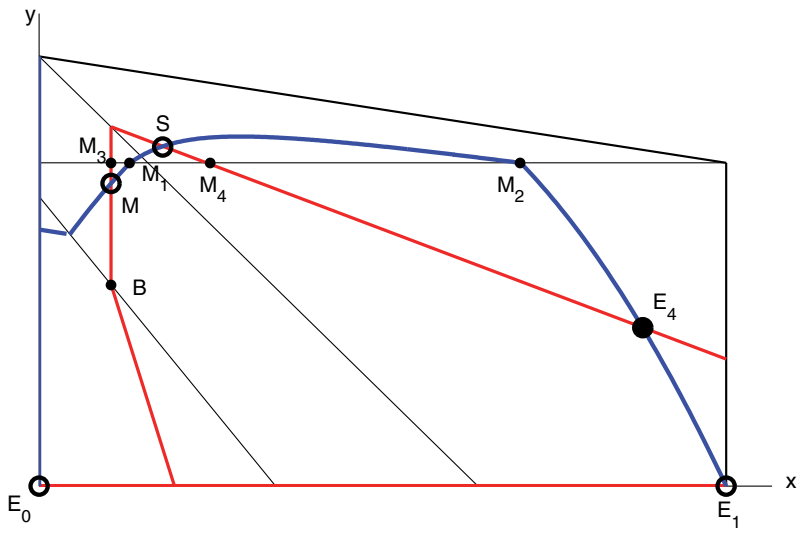

Figure 3. *The nullclines and notations for* $0.016204 < P < 0.028408$.

know the relative position relationship among some intersections (see Figure 3). Denote the intersections of the parabola $y = g(x)$ and the straight line $y = \frac{100}{3}P - 0.19$ as M_1 (left) and M_2 (right). That is

$$M_i(x_{M_i}, y_{M_i}) \quad (i = 1, 2) : \begin{cases} y = \dfrac{10}{81}(3 - 2x)(1 + 4x), \\ y = \dfrac{100}{3}P - 0.19. \end{cases}$$

Hence

$$\begin{cases} x_{M_1} = 0.625 - \sqrt{0.958 - 33.75P}, \\ y_{M_1} = \dfrac{100}{3}P - 0.19, \end{cases}$$

and

$$\begin{cases} x_{M_2} = 0.625 + \sqrt{0.958 - 33.75P}, \\ y_{M_2} = \dfrac{100}{3}P - 0.19. \end{cases}$$

Denote by M_3 the intersection of the straight line $x = 0.157035$ and $y = \frac{100}{3}P - 0.19$, i.e., the coordinate of M_3 is

$$x_{M_3} = 0.157035, \quad y_{M_3} = \frac{100}{3}P - 0.19.$$

Denote by M_4 the intersection of the straight line $x + 3.24y = 108P - 0.25$ and $y = \frac{100}{3}P - 0.19$.

That is,

$$M_4(x_{M_4}, y_{M_4}) : \begin{cases} x + 3.24y = 108P - 0.25, \\ y = \dfrac{100}{3}P - 0.19, \end{cases} \Rightarrow \begin{cases} x_{M_4} = 0.3656, \\ y_{M_4} = \dfrac{100}{3}P - 0.19. \end{cases}$$

Denote by M the intersection of the straight line $x = 0.157035$ and the parabola $y = g(x)$. That is,

$$y_M = g(0.157035) = 0.539885.$$

Denote by B the intersection of the straight line $x = 0.157035$ and $x + y = \frac{100}{3}P - \frac{1}{4}$, i.e., the y-coordinate of B is

$$y_B = \frac{100}{3}P - 0.407035.$$

Denote by S the intersection of the hyperbola Γ_2 and the straight line $x+3.24y = 108P-0.25$. That is,

$$S(x_S, y_S) : \begin{cases} \dfrac{19x}{5000P - 150y} + \dfrac{27y}{10 + 40x} = 1, \\ x + 3.24y = 108P - 0.25, \end{cases}$$

$$\Rightarrow \begin{cases} x_S = 28.197845P - 0.378582, \\ y_S = 24.630295P + 0.039686. \end{cases} \tag{3.3}$$

Denote by E_4 the intersection (the right one) of the parabola $y = g(x)$ and the straight line $x + 3.24y = 108P - 0.25$. That is,

$$E_4(x_{E_4}, y_{E_4}) : \begin{cases} y = \dfrac{10}{81}(3 - 2x)(1 + 4x), \\ x + 3.24y = 108P - 0.25, \end{cases}$$

$$\Rightarrow \begin{cases} x_{E_4} = \dfrac{25}{32} + \dfrac{3}{32}\sqrt{121 - 3840P}, \\ y_{E_4} = g(x_{E_4}). \end{cases} \tag{3.4}$$

According to the relative position relationship about these intersection points $M, M_1, M_2, M_3, M_4, E_4$, the case is divided into four subcases depending on the range of P:

(i) $0.016204 < P < 0.018995$;
(ii) $0.018995 \le P < 0.021897$;
(iii) $0.021897 \le P < 0.026391$;
(iv) $0.026391 \le P < 0.028408$.

We analyze these four subcases in Appendix C and arrive at the following result.

Theorem 3.3. *When* $0.016204 < P < 0.028408$, *the boundary equilibria of system* (3.1)–(3.2) *are unstable saddles. For the stability of the internal equilibria, there are three cases:*

If $0.016204 < P < 0.018995$, *then the system has one internal equilibrium* E_4, *which is a GAS node;*

If $0.018995 < P < 0.028408$, *then the system has three internal equilibria* E_2, E_3, E_4. E_2 *is an unstable equilibrium,* E_3 *is a saddle, and* E_4 *is an LAS node;*

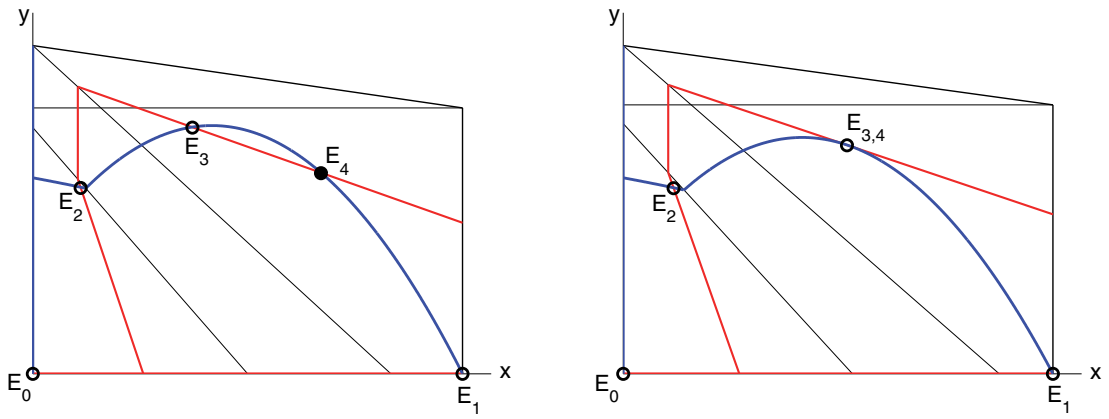

(a) $0.028408 < P < 0.031510$. (b) $P = 0.031510$.

Figure 4. *The nullclines and equilibria for* $0.028408 < P \leq 0.031510$.

If $P = 0.018995$*, then the system has two internal equilibrium* $E_{2,3}, E_4$*.* E_4 *is a stable node,* $E_{2,3}$ *is an unstable saddle node. Moreover, the system has no limit cycle.*

3.2.3. Case 3: $0.028408 \leq P \leq 0.031510$. In this case, the x-nillcline is joint with two parts: one is the parabola $y = g(x)$, and the other is a hyperbola Γ_1. If $x_{A_1} < 0.157035$, that is,

$$\frac{1}{160}\left[181 - \sqrt{48841 - 864000P}\right] < 0.157035,$$

which is equivalent to $P < 0.028408$, then the original system has no internal equilibria in the domain $\{(x, y) \in \Omega : x + y < \frac{100}{3}P - \frac{1}{4}\}$. In other words, when $0.028408 < P < 0.031510$, the system has three internal equilibria E_2, E_3, E_4, and the equilibrium E_2 lies below the line $x + y = \frac{100}{3}P - \frac{1}{4}$. The other equilibria E_3, E_4 lie above the line $0.8x + y = \frac{100}{3}P$ (see Figure 4(a)). The equilibrium E_3 is an unstable saddle and E_4 is an LAS node, which are the same as those in the previous case. The equilibrium E_2 is the intersection of the hyperbola Γ_1 and straight line $2.592x + y = \frac{100}{3}P$ in the domain $\{(x, y) \in \Omega : x + y < \frac{100}{3}P - \frac{1}{4}\}$. By simple calculations, we obtain the coordinates of E_2:

$$\begin{cases} x_{E_2} = 1.25625 - \sqrt{1.5781640 - 13.020833P}, \\ y_{E_2} = \dfrac{100}{3}P - 2.592x_{E_2}. \end{cases} \tag{3.5}$$

Now we analyze the stability of E_2. At E_2, since $-\frac{F_x}{F_y} > -\frac{G_x}{G_y}, F_x < 0, F_y < 0, G_x > 0, G_y > 0$, we have

$$\operatorname{sign}\big(\operatorname{Det}J(E_2)\big) = \operatorname{sign}\left(-\frac{F_x}{F_y} - \left(-\frac{G_x}{G_y}\right)\right) > 0,$$

$$\operatorname{sign}\big(\operatorname{Tr}J(E_2)\big) = \operatorname{sign}\big(xF_x + yG_y\big) = \operatorname{sign}\left(-\frac{4}{5} + \frac{1620y}{(\frac{5000}{3}P - 50y)^2}\right).$$

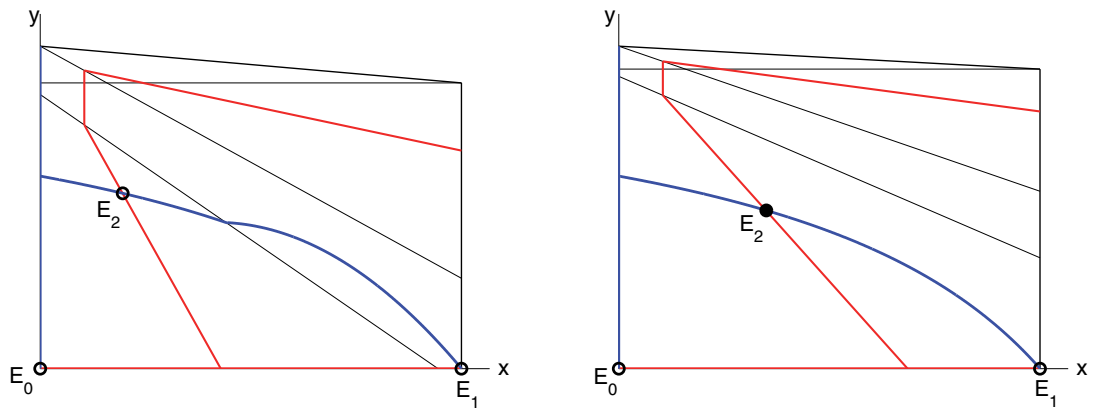

(a) $0.031510 < P < 0.058622$. (b) $0.058622 < P < 0.116640$.

Figure 5. *The nullclines and equilibria for* $0.031510 < P < 0.116640$.

Define

$$h(P) = -\frac{4}{5} + \frac{1620y}{(\frac{5000}{3}P - 50y)^2},$$

where $y = y_{E_2}$ which is determined by (3.5). $h(P) = 0$, thus $P = 0.058652$. Note that $h(P)$ is a monotone decreasing function, therefore, when $P < 0.058652$, $\mathrm{sign}(\mathrm{Tr}J(E_2)) > 0$, and the equilibrium E_2 is an unstable node. Otherwise, when $P > 0.058652$, $\mathrm{sign}(\mathrm{Tr}J(E_2)) < 0$, and the equilibrium E_2 is an LAS node if it exists. Obviously, the equilibrium E_2 is an unstable node in this case.

When $P = 0.031510$, the system has two internal equilibria $E_2, E_{3,4}$ (see Figure 4(b)). When P tends to 0.031510 from the left, E_3 and E_4 collide and become $E_{3,4}$ which lies on the line $0.8x + y = \frac{100}{3}P$. Since E_3 is an unstable saddle and E_4 is an LAS node, the equilibrium $E_{3,4}$ is an unstable saddle node, and a saddle-node bifurcation occurs.

3.2.4. Case 4: $0.031510 < P < 0.116640$. In this case, the system has one internal equilibrium E_2, whose stability has three cases with different signs of $\mathrm{Tr}J(E_2)$.

If $0.031510 < P < 0.058622$, then $\mathrm{Det}J(E_2) > 0$ and $\mathrm{Tr}J(E_2) > 0$, thus the E_2 is an unstable node (see Figure 5(a)). Since the system has a unique internal equilibrium E_2, and E_2 is an unstable node, the system has at least one limit cycle by the Poincaré–Bendixson theorem.

If $P = 0.058622$, then $\mathrm{Det}J(E_2) > 0$ and $\mathrm{Tr}J(E_2) = 0$. The Jacobian matrix $J(E_2)$ has a pair of pure imaginary eigenvalues and the internal equilibrium E_2 is a center-type equilibrium.

If $0.058622 < P < 0.116640$, then $\mathrm{Det}J(E_2) > 0$ and $\mathrm{Tr}J(E_2) < 0$, which shows that the equilibrium E_2 is a stable node (see Figure 5(b)). The system has no limit cycle, the boundary equilibria E_0, E_1 are unstable saddles. There exists a heteroclinic orbit connecting E_1 and E_2, so E_2 is a GAS node.

3.2.5. Case 5: $0.116640 \le P \le 0.121203$. When $0.116640 < P < 0.121203$, the system has two internal equilibria E_2 and E_5 (see Figure 6). The coordinates of these equilibria

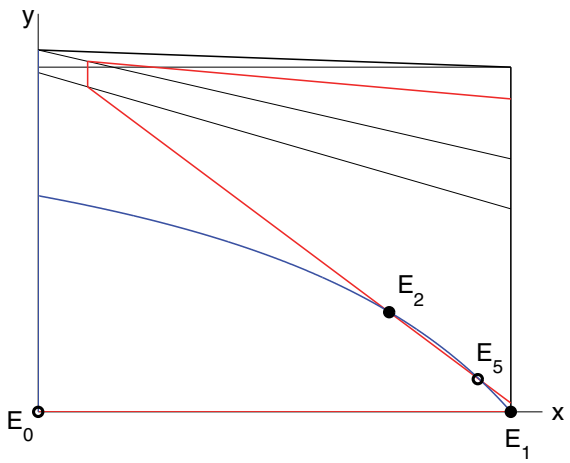

Figure 6. *The nullclines and equilibria for* $0.116640 < P < 0.121203$.

are determined by the equations

$$xy - \frac{100}{3}Px - \frac{201}{80}y + 50P = 0,$$
$$2.592x + y - \frac{100}{3}P = 0.$$

The coordinates of E_2 are

$$\left(x_{E_2} = 1.25625 - \sqrt{1.578164 - 13.020833P}, \quad y_{E_2} = \frac{100}{3}P - 2.592x_{E_2}\right)$$

and the coordinates of E_5 are

$$\left(x_{E_5} = 1.25625 + \sqrt{1.578164 - 13.020833P}, \quad y_{E_5} = \frac{100}{3}P - 2.592x_{E_5}\right).$$

The equilibrium E_2 is an LAS node since $\mathrm{Det}J(E_2) > 0$, $\mathrm{Tr}J(E_2) < 0$. To determine the local stability of the equilibrium E_5, we consider the Jacobian matrix of the original system at E_5:

$$J(E_5) = \begin{pmatrix} xF_x(x,y) & xF_y(x,y) \\ yG_x(x,y) & yG_y(x,y) \end{pmatrix}.$$

Since $-\frac{F_x}{F_y} < -\frac{G_x}{G_y}$, $F_x < 0$, $F_y < 0$, $G_x > 0$, and $G_y > 0$, we see that

$$\mathrm{sign}\big(\mathrm{Det}J(E_5)\big) = \mathrm{sign}\left(-\frac{F_x}{F_y} - \left(-\frac{G_x}{G_y}\right)\right) < 0,$$

which implies that E_5 is an unstable saddle.

If $P = 0.116640$, the system has one internal equilibrium E_2. When P tends to 0.116640 from the right, E_5 collides with E_1 and becomes the equilibrium $E_{1,5}$ which lies on the x-axis; transcritical bifurcation occurs.

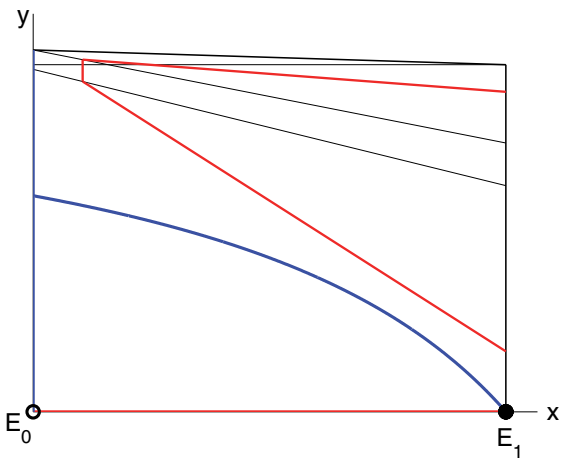

Figure 7. *The nullclines and equilibria for* $0.121203 < P < 0.2$.

If $P = 0.121203$, the system has one internal equilibrium $E_{2,5}$. When P tends to 0.121203 from the left, E_2 and E_5 collide and become the equilibrium $E_{2,5}$, which shows that a saddle-node bifurcation occurs and $E_{2,5}$ is a stable saddle node, since E_2 is a stable node and E_5 is a saddle.

3.2.6. Case 6: $0.121203 < P < 0.2$. The system has only the boundary equilibria E_0 and E_1; E_0 is a saddle and E_1 is a GAS node. No internal equilibria exist in this case (see Figure 7). All orbits in Ω tend to E_1, which implies that the grazer will go extinct despite high food abundance.

3.3. Bifurcation diagram. In Figure 8, we accurately plot the bifurcation diagram with respect to the total mass of phosphorus in the entire system according to the results of our mathematical analysis from the previous section. Specifically, we have established the following:

- When $0 < P \leq 0.016204$, there exist no internal equilibria and the boundary equilibrium E_1 is GAS.
- When $0.016204 < P < 0.018995$, there exists a unique internal equilibrium E_4 which is GAS, and all boundary equilibria are unstable saddle.
- When $P = 0.018995$, there exist two internal equilibria: E_4 and $E_{2,3}$. E_4 is GAS, $E_{2,3}$ is an unstable saddle node.
- When $0.018995 < P < 0.031510$, there exist three internal equilibria: E_2 is an unstable node, E_3 is an unstable saddle, and E_4 is LAS.
- When $P = 0.031510$, there exist two internal equilibria: E_2 is an unstable node and $E_{3,4}$ is a saddle node.
- When $0.031510 < P < 0.058622$, there exists a unique internal equilibrium E_2 which is an unstable node and there exists a limit cycle.
- When $0.058622 < P \leq 0.116640$, there exists a unique internal equilibrium E_2 which is GAS.

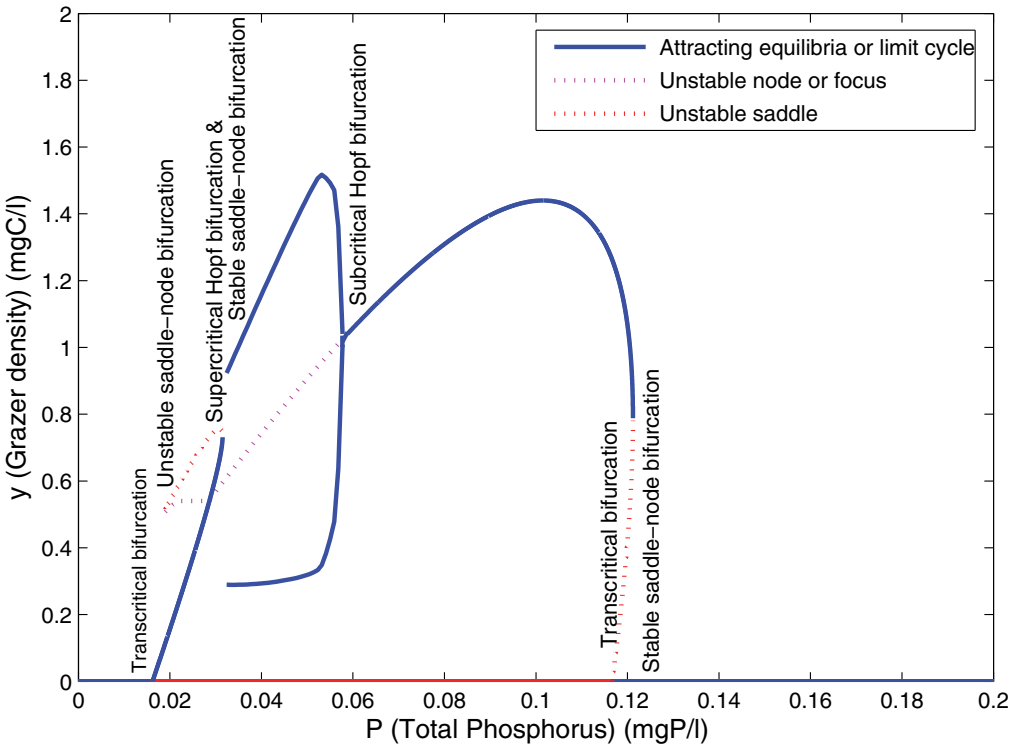

Figure 8. *Bifurcation diagram for the knife-edge system* (3.1)–(3.2) *of the grazer. The bifurcation parameter, P, varies from* 0 *to* 0.2 *mgP/l.*

- When $0.116640 < P < 0.121203$, there exist two internal equilibria: E_2 is LAS, E_5 is a saddle; the boundary equilibrium E_1 is LAS, all solutions either tend to the internal equilibrium E_2 or tend to the boundary equilibrium E_1 (bistability).
- When $P = 0.121203$, there exists one internal equilibrium $E_{2,5}$, which is a stable saddle node.
- When $P > 0.121203$, there exist no internal equilibria and the boundary equilibrium E_1 is GAS.

The above bifurcation analysis exhibits that almost all known types of local bifurcations occur in this model: transcritical bifurcation (at $P = 0.016204, 0.116640$), saddle-node bifurcation (at $P = 0.018995, 0.030510, 0.121203$), supercritical Hopf bifurcation (at $P = 0.031510$), subcritical Hopf bifurcation (at $P = 0.058622$). The bifurcation phenomenon is more complicated at $P = 0.031510$. As P passes through this value, the internal stable equilibrium disappears via saddle-node bifurcation, at least a limit cycle occurs, and all solutions may tend to such a limit cycle via supercritical Hopf bifurcation; thus both supercritical Hopf bifurcation and saddle-node bifurcation occur at this value of P. We would like to emphasize that our bifurcation diagram is generated and guaranteed by our mathematical analysis, whereas most bifurcation diagrams generated by existing software such as XPPAUT are approximations.

The nonsmooth model in this paper is prone to cause numerical errors, thus it is necessary to provide mathematical confirmation.

4. Discussion. The stoichiometric knife-edge model proposed by Peace et al. [28] consists of three minimum functions which is more than the other existing two species stoichiometric models. Therefore, it is more challenging to perform systematic mathematical analysis. For a fixed set of parameters (except P), we provide a rigorous and almost complete mathematical analysis for local and global stability results of all equilibria, the existence of limit cycles, and a rigorous bifurcation analysis with respect to the total phosphorus parameter P. Our bifurcation analysis reveals very rich dynamics generated by this model. Almost all types of local bifurcations occur in this model. At one bifurcation value of the parameter P, both supercritical Hopf bifurcation and saddle-node bifurcation occur simultaneously. Our analysis also exhibits the existence of bistability when $0.116640 < P < 0.121203$.

This knife-edge model is modified from the LKE model by explicitly incorporating the impact of excess nutrient content. To compare the dynamics of these two models, we recall the LKE model below [19]:

$$\frac{dx}{dt} = bx\left(1 - \frac{x}{\min\{K, (P-\theta y)/q\}}\right) - f(x)y, \tag{4.1}$$

$$\frac{dy}{dt} = e\min\left\{1, \frac{(P-\theta y)/x}{\theta}\right\} f(x)y - dy. \tag{4.2}$$

Intuitively, we affirm that if the total phosphorus is not at an extremely high concentration, these two models lead to almost the same dynamics. If the total phosphorus is at an extremely high concentration, their dynamics are quite different. To illustrate this idea, we perform numerical experiments. Our simulations use the Holling type-II function $f(x) = \frac{cx}{a+x}$ for the grazer's ingestion rate and parameter values stated in section 3. We start with the same initial conditions $x_0 = 0.5$ mgC/l, $y_0 = 0.25$ mgC/l for all simulations.

Solutions of the knife-edge model are compared to those of the LKE model for various P values (representing nutrient availability) in Figure 9. For small P (panels (a) and (b) in Figure 9), they have similar qualitative behaviors and slightly different quantitative behaviors; panel (a) shows positive stable equilibrium and panel (b) shows periodic oscillations around an unstable equilibrium. However, for large P (panels (c) and (d) in Figure 9), they are completely different; panel (c) shows an attractive internal equilibrium and panel (d) shows the grazer's extinction for the knife-edge model. The solutions of the LKE model in panels (c) and (d) are similar to those in panel (b), oscillating around an unstable equilibrium. Interestingly, when P is near the supercritical Hopf bifurcation value ($P = 0.031510$) for the knife-edge model, they are completely different (see Figure 10). Near this bifurcation value, the sensitivity of the solution for the knife-edge model is very high with respect to the parameter P.

We also compare the solutions of these two models for various K values (representing light intensity). Simulations of these models are presented in Figure 11 for varying values of K. Differences between the two solutions are first illustrated in panel (a): for small K, the grazer goes extinct for the knife-edge model, while the solution of the LKE model exhibits an attractive internal equilibrium. For intermediate K values (panels (b) and (c) in Figure 11), the

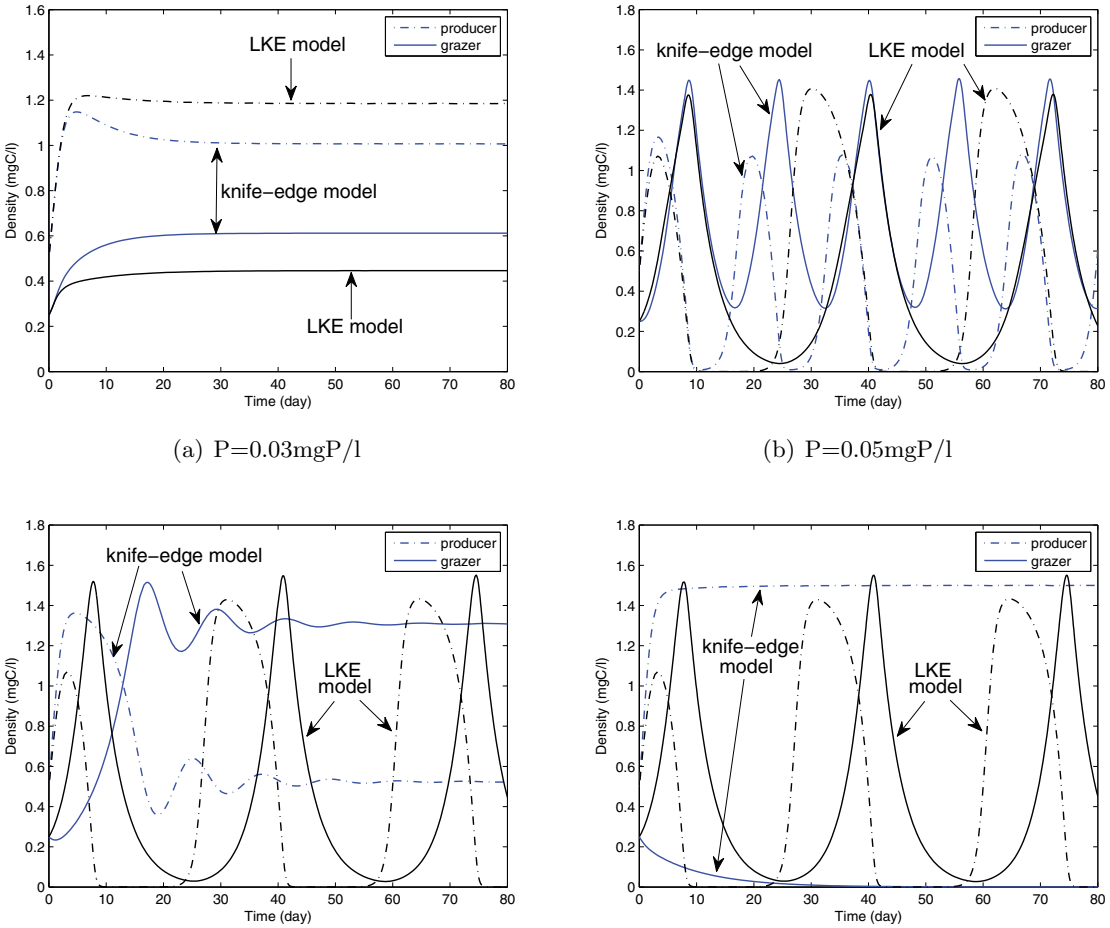

(a) P=0.03mgP/l (b) P=0.05mgP/l

(c) P=0.08mgP/l (d) P=0.2mgP/l

Figure 9. *Comparison of the knife-edge model and the LKE model with different total phosphorus. Numerical simulations of these two models performed using parameter values stated in section 3 and varying values for P. The initial conditions are* $x_0 = 0.5mgC/l$, $y_0 = 0.25mgC/l$. *Grazer and producer densities are depicted by solid and dash-dotted lines, respectively. The solutions of the knife-edge model and the LKE model are plotted by blue and black lines, respectively.*

solutions in both models have similar qualitative behaviors and slightly different quantitative behaviors: panel (b) shows an attractive internal equilibrium and panel (c) shows periodic oscillations around an unstable equilibrium. For large K (panel (d) in Figure 11), the grazer goes extinct for the LKE model, while the solution of the knife-edge model exhibits an attractive internal equilibrium. Furthermore, similar to the previous simulations, there exists a special value $K = 0.98$ as the subcritical Hopf bifurcation of the LKE model. Near this bifurcation value, solutions of the knife-edge model and that of the LKE model are completely different (see Figure 12), which implies that the sensitivity of the solution with respect to the parameter K is high when K is near this bifurcation value.

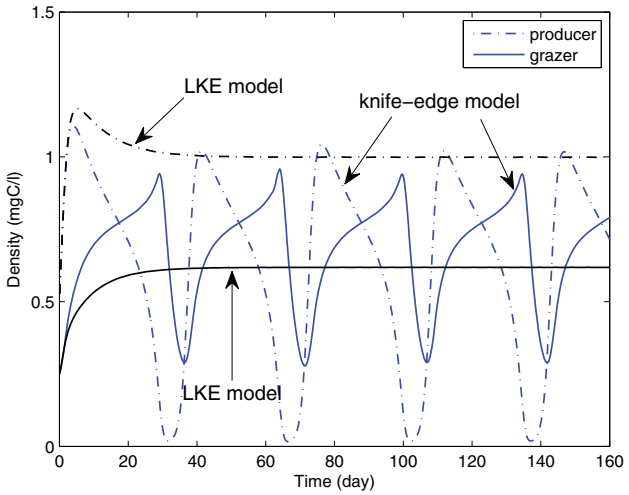

Figure 10. *Comparison of the knife-edge model and the LKE model with* $P = 0.033mgP/l$.

In some sense, our work presents a series of rather complex snapshots of the stoichiometric knife-edge model proposed by Peace et al. [28] with its dynamics initially studied in [27]. A full mathematical analysis of the model dynamics that covers all possible parameter values remains a challenge and is highly desirable. Although we have shown existence and nonexistence of limit cycles for all possible cases in this paper, we have not shown the uniqueness or nonuniqueness of limit cycles. These questions are daunting with the nonsmoothness of the model, and we leave these intriguing mathematical questions for future studies.

Due to the high sensitivities of the stoichiometric knife-edge-type model (1.1)–(1.2) with respect to key parameters P and K, in real applications, some suitable data assimilation methods may be needed to enhance the model's prediction capability. Data assimilation refers to methods for updating initial conditions of a highly sensitive dynamical model by combining recent data with prior forecasts. Kostelich et al. applied a modern state estimation algorithm (the local ensemble transform Kalman filter), previously developed for numerical weather prediction, to two different mathematical models of glioblastoma, taking into account likely errors in model parameters and measurement uncertainties in magnetic resonance imaging [12]. Their mathematical methodology may be useful for other modeling efforts in biology and oncology [22].

Appendix A. Dissipativity.

Proof of Theorem 2.1. We only prove the invariance for the case $k = K$, since the other case $k = P/q$ is simpler to prove. The positive x-axis and the positive y-axis are both invariant. On the right boundary of Ω, $x = k, 0 \le y \le P - qK$, we have $\frac{dx}{dt} = -\min\{\frac{1}{a+k}, \frac{1}{P-y}\}ky < 0$; therefore, all orbits starting from Ω cannot escape Ω from these three boundaries. To show that solutions starting from Ω cannot escape Ω from the upper boundary, we can define

$$u = qx + y.$$

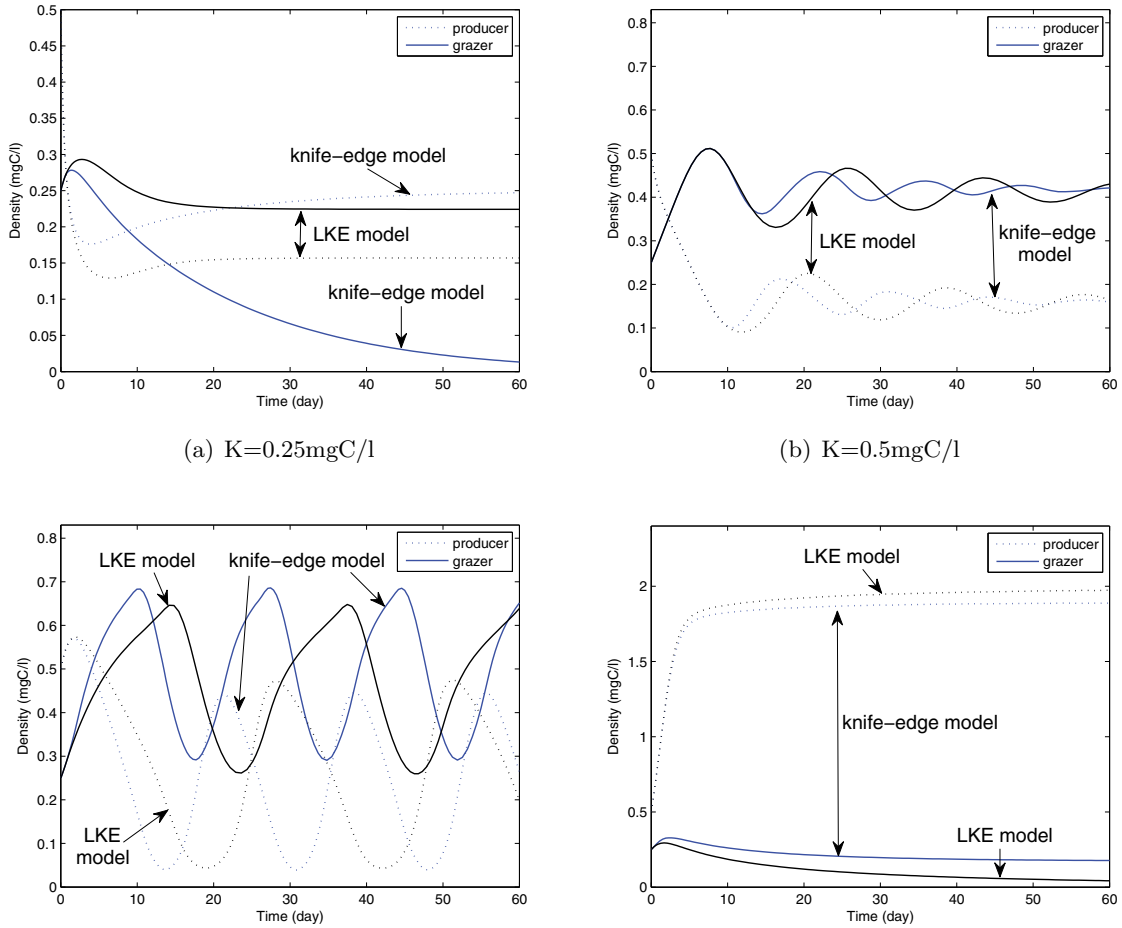

Figure 11. *Comparison of the knife-edge model and the LKE model with different carrying capacities. Numerical simulations of these two models performed using parameter values stated in section 3 except* $P = 0.025$ *mgP/l and with varying values for K. The initial conditions are* $x_0 = 0.5mgC/l$, $y_0 = 0.25mgC/l$. *Grazer and producer densities are depicted by solid and dotted lines, respectively. The solutions of the knife-edge model and the LKE model are plotted by blue and black lines, respectively.*

Then on the upper boundary,

$$qx + y = P, \quad 0 \le x \le k,$$

we have

$$\frac{du}{dt} = q\frac{dx}{dt} + \frac{dy}{dt} = qx\left(b\left(1 - \frac{qx}{P-y}\right) - \frac{y}{a+x}\right) + y\left(\frac{P-y}{a+x} - d\right) = -dy < 0,$$

which shows that all orbits stating from Ω will stay in Ω for all forward times. ■

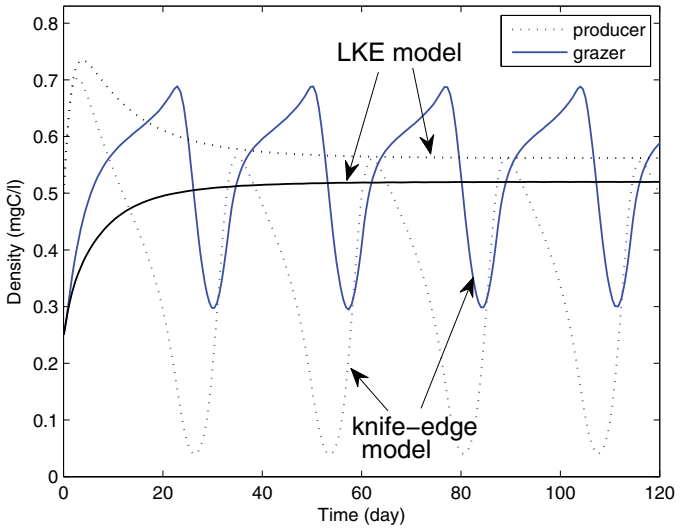

Figure 12. *Comparison of the knife-edge model and the LKE model with* $K = 0.99 mgC/l$.

Appendix B. Boundary stability.

Proof of Theorem 2.2. To determine the local stability of the equilibria $E_0 = (0, 0)$ and $E_1 = (k, 0)$, we compute the Jacobian matrices through F, G and their partial derivatives. The partial derivatives of these functions exist almost everywhere on Ω:

$$F_x = \begin{cases} -\frac{b}{K} + \frac{y}{(a+x)^2}, & x+y > P-a, y < P-qK, \\ -\frac{b}{K}, & x+y < P-a, y < P-qK, \\ -\frac{bq}{P-y} + \frac{y}{(a+x)^2}, & x+y > P-a, y > P-qK, \\ -\frac{bq}{P-y}, & x+y < P-a, y > P-qK; \end{cases}$$

$$F_y = \begin{cases} -\frac{1}{a+x}, & x+y > P-a, y < P-qK, \\ -\frac{P}{(P-y)^2}, & x+y < P-a, y < P-qK, \\ -\frac{bqx}{(P-y)^2} - \frac{1}{(a+x)^2}, & x+y > P-a, y > P-qK, \\ -\frac{P+bqx}{(P-y)^2}, & x+y < P-a, y > P-qK; \end{cases}$$

$$G_x = \begin{cases} \frac{ae}{(a+x)^2}, & ex+y < P, x+y > P-a, \\ -\frac{P-y}{(a+x)^2}, & ex+y > P, ex(a+x) > (P-y)^2, \\ \frac{e}{P-y}, & x+y < P-a, ex(a+x) < (P-y)^2; \end{cases}$$

$$G_y = \begin{cases} 0, & ex+y < P, x+y > P-a, \\ -\frac{1}{a+x}, & ex+y > P, ex(a+x) > (P-y)^2, \\ \frac{ex}{(P-y)^2}, & x+y < P-a, ex(a+x) < (P-y)^2. \end{cases}$$

The Jacobian matrix of system (2.1)–(2.2) is

$$J(x,y)=\begin{pmatrix} F(x,y)+xF_x(x,y) & xF_y(x,y) \\ yG_x(x,y) & G(x,y)+yG_y(x,y) \end{pmatrix}.$$

At the origin, $F(0,0)=b, G(0,0)=-d$, it takes the form

$$J(E_0)=\begin{pmatrix} b & 0 \\ 0 & -d \end{pmatrix}.$$

Therefore, the origin is always unstable in the form of a saddle, whose stable manifold is the y-axis and unstable manifold is the x-axis.

At E_1, since $F(k,0)=0, F_x(k,0)=-b/k$, the Jacobian matrix is

$$J(E_0)=\begin{pmatrix} -b & kF_y(k,0) \\ 0 & G(k,0) \end{pmatrix}.$$

We see that if $G(k,0)>0$, then E_1 is an unstable saddle; if $G(k,0)<0$, then E_1 is an LAS node.

Next, we start to analyze the sign of $G(k,0)$.

When $P<qK$, then $k=P/q$. According to the model assumptions (ii) and (iii) at the beginning of section 2, $q<e<1$. This implies that $ek>qk=P$ and hence $k>P$. Thus

$$G(k,0)=\frac{P}{a+k}-d=\frac{P(q-d)-adq}{aq+p}.$$

Therefore, we see that if $q-d<0$ or $P<adq/(q-d)$, then $G(k,0)<0$.

When $P>qK$, i.e., $k=K$, the $G(k,0)$ have the following form:

$$G(k,0)=G(K,0)=\begin{cases} \frac{eK}{a+K}-d, & eK\le P\le a+K, \\ \frac{P}{a+K}-d, & p<eK, \\ \frac{eK}{P}-d, & P>a+K. \end{cases}$$

We have the following conclusions:

If $eK\le P\le a+K$ and $eK-d(a+K)<0$, then $G(K,0)<0$.

If $P<eK$ and $P<d(a+K)$, then $G(K,0)<0$.

If $P>a+K$ and $P>eK/d$, then $G(K,0)<0$. ∎

Appendix C. Global stability.

Proof of Theorem 3.3. (i) When $0.016204<P<0.018995$, we have $x_{M_1}<0, x_S<x_{M_3}$, and $x_{M_4}<x_{M_2}<x_{E_4}<1.5$. The system has one internal equilibrium E_4 which lies in the domain $\{(x,y)\in\Omega: y<\frac{100}{3}P-0.19, 0.8x+y>\frac{100}{3}P\}$. The coordinate of E_4 is determined by (3.4). To determine the local stability of the equilibrium E_4, we consider the Jacobian matrix of system (3.1)–(3.2); at E_4, it takes the form

$$J(E_4)=\begin{pmatrix} xF_x(x,y) & xF_y(x,y) \\ yG_x(x,y) & yG_y(x,y) \end{pmatrix}$$

with $x = x_{E_4}$, $y = y_{E_4}$. Since $-\frac{F_x}{F_y} < -\frac{G_x}{G_y} < 0, F_y < 0, G_x < 0, G_y < 0$, we see that $F_x < 0$ and

$$\begin{aligned}\operatorname{sign}\big(\operatorname{Det}J(E_4)\big) &= \operatorname{sign}\big(F_xG_y - F_yG_x\big)\\ &= \operatorname{sign}\left(\frac{F_xG_y - F_yG_x}{F_yG_y}\right)\\ &= \operatorname{sign}\left(-\frac{G_x}{G_y} - \left(-\frac{F_x}{F_y}\right)\right) > 0\end{aligned}$$

and

$$\operatorname{sign}\big(\operatorname{Tr}J(E_4)\big) = \operatorname{sign}\big(xF_x + yG_y\big) < 0.$$

Hence, E_4 is an LAS. In addition,

$$\begin{aligned}\triangle J(E_4) &= \big(\operatorname{Tr}J(E_4)\big)^2 - 4\operatorname{Det}J(E_4)\\ &= \big(xF_x + yG_y\big)^2 - 4xy(F_xG_y - F_yG_x)\\ &= (xF_x - yG_y)^2 + 4xyF_yG_x > 0,\end{aligned}$$

which shows that E_4 is an LAS node. Since the boundary equilibria E_0 and E_1 are unstable saddles, all orbits in Ω tend to E_4, thus E_4 ia a GAS node.

(ii) When $0.018995 < P < 0.021897$, we have $x_{M_1} < x_{M_3} < x_S < x_{M_4} < x_{M_2} < x_{E_4} < 1.5$, the system has three internal equilibria E_2, E_3, E_4, and the equilibria E_2, E_3 lie above the line $y = \frac{100}{3}P - 0.19$; the other equilibrium E_4 lies below this line. The local stability of the equilibrium E_4 is completely the same as that in the subcase (i), which is an LAS node. The x-coordinate of E_2 is $x_{E_2} = 0.157035$. Since the equilibrium E_2 lies on the hyperbola $\Gamma_2 : \frac{19x}{5000P-150y} + \frac{27y}{10+40x} = 1$, the y-coordinate is

$$y_{E_2} = 16.666667P - \sqrt{277.777778P^2 - 10.050249P + 0.102901} + 0.301507.$$

The equilibrium E_3 and point S are the same one in this case, thus the coordinate of E_3 is

$$\begin{aligned}x_{E_3} &= 28.197845P - 0.378582,\\ y_{E_3} &= 24.630295P + 0.039686.\end{aligned}$$

To determine the local stability of E_2, E_3, we also consider the Jacobian matrix as we did in the previous subcase. At E_2, since $-\frac{F_x}{F_y} > 0, F_y < 0, G_x > 0, G_y = 0$, then $F_x > 0$,

$$\operatorname{sign}\big(\operatorname{Det}J(E_2)\big) = \operatorname{sign}\big(-F_yG_x\big) > 0,$$

and

$$\operatorname{sign}\big(\operatorname{Tr}J(E_2)\big) = \operatorname{sign}\big(xF_x\big) > 0.$$

Hence, E_2 is an unstable node or focus. From the topological point of view, the node and focus with same stability are topologically equivalent; therefore, we can treat the equilibrium E_2 as an unstable node.

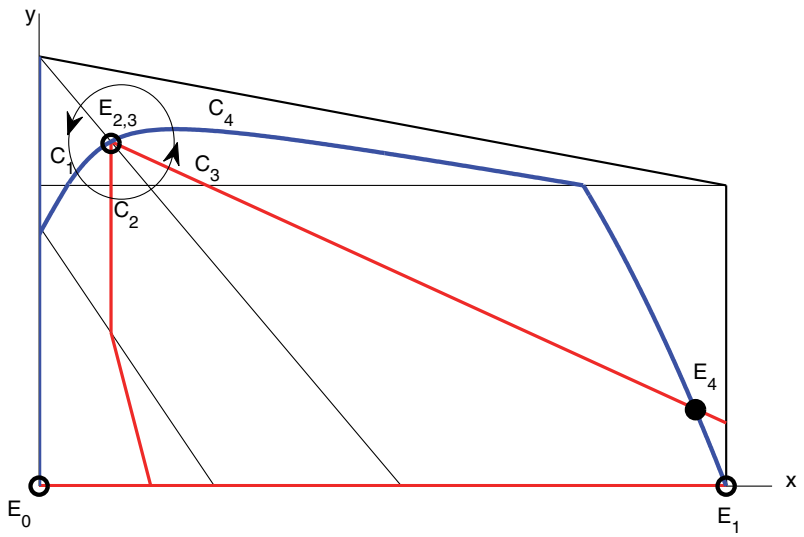

Figure 13. *The nullcines and equilibria for* $P = 0.018995$.

At E_3, since $-\frac{F_x}{F_y} > -\frac{G_x}{G_y}, F_y < 0, G_x < 0, G_y < 0$, then

$$\text{sign}\big(\text{Det}J(E_3)\big) = \text{sign}\big(F_xG_y - F_yG_x\big) = \text{sign}\left(-\frac{G_x}{G_y} - \left(-\frac{F_x}{F_y}\right)\right) < 0.$$

Hence, E_3 is an unstable saddle.

If $P = 0.018995$, then the system has two internal equilibria $E_{2,3}, E_4$; when P tends to 0.018995 from the right, E_2 and E_3 collide and become the equilibrium $E_{2,3}$, which lies on the line $0.8x + y = \frac{100}{3}P$. Since E_2 is an unstable node, E_3 is an unstable saddle. Therefore, the equilibrium $E_{2,3}$ is an unstable saddle node. E_4 is an LAS node. Next, we show that the system has no limit cycle in this case. Suppose that the system has a nontrivial periodic solution $\Gamma : (x(t), y(t))$ in Ω. Since the system has two internal equilibria $E_{2,3}, E_4$, at least one of them lies inside the domain bounded by the closed orbit Γ. We only consider the equilibrium $E_{2,3}$ lying inside this domain since the other two cases can be proven similarly. Obviously, Γ must intersect the x-nullcline and y-nullcline. We let the intersections of Γ and the x-nullcline be C_1 (left) and C_4 (right); and let the intersections of Γ and the y-nullcline be C_2 (left) and C_3 (right)(see Figure 13). Since $\frac{dx}{dt} < 0$ above the x-nullcline Γ_2, then the orbit Γ is in the counterclockwise direction. On the other hand, since $\frac{dy}{dt} < 0$ above the y-nullcline $x + 3.24y = \frac{100}{3}P - \frac{1}{4}$, we see that the y-coordinate of the point C_3 must be larger than that of the point C_4, which is a contradiction since the x-nullcline is above the y-nullcline $x + 3.24y = \frac{100}{3}P - \frac{1}{4}$ between $E_{2,3}$ and E_4. In addition, since the boundary equilibria E_0, E_1 are an unstable saddle in this case, there exists a heteroclinic orbit connecting the equilibria $E_{2,3}$ and E_4; E_4 is a GAS node.

(iii) When $0.021897 < P < 0.026391$, we have $x_{M_3} < x_{M_1} < x_S < x_{M_4} < x_{M_2} < x_{E_4} < 1.5$, and $y_B < y_M < \frac{100}{3}P - 0.19$. The system has three internal equilibria E_2, E_3, and E_4. The

equilibrium E_3 lies above the line $y = \frac{100}{3}P - 0.19$; the other equilibria E_2, E_4 lie below this line. The stability of the equilibria E_3 and E_4 is the same as those in the previous subcase: the equilibrium E_3 is an unstable saddle and E_4 is an LAS node. E_2 is an intersection point of the parabola $y = g(x)$ and a straight line $x = 0.157035$ and its coordinates are

$$x_{E_2} = 0.157035, \quad y_{E_2} = g(x_{E_2}) = 0.539885.$$

Since $-\frac{F_x}{F_y} > 0, F_y < 0, G_x > 0, G_y = 0$, we have $F_x > 0$, $\text{sign}(\text{Det}J(E_2)) > 0$, and $\text{sign}(\text{Tr}J(E_2)) > 0$; hence E_2 is also an unstable node. The stability of E_2 is the same as that in the previous subcase. Therefore $P = 0.021897$ is not a bifurcation value.

(iv) When $0.026391 \le P < 0.028408$, we have $x_{M_4} < x_{M_1} < x_{M_2} < x_{E_4} < 1.5$, and $y_M > y_B$. The system has three internal equilibria E_2, E_3, E_4 that lie below the line $y = \frac{100}{3}P - 0.19$. In other words, the system has no internal equilibria in the domain $\{(x, y) \in \Omega : y > \frac{100}{3}P - 0.19\}$ in this subcase. The stability of the equilibria E_2 and E_4 is the same as those in the previous subcase. The equilibrium E_2 is an unstable node and E_4 is an LAS node. E_3 is a left intersection of the parabola $y = g(x)$ and the straight line $x + 3.24y = 108P - 0.25$. Its coordinates are

$$x_{E_3} = \frac{25}{32} - \frac{3}{32}\sqrt{121 - 3840P}, \quad y_{E_3} = g(x_{E_3}).$$

Since $-\frac{F_x}{F_y} > -\frac{G_x}{G_y}, F_y < 0, G_x < 0, G_y < 0$, we see that

$$\text{sign}\big(\text{Det}J(E_3)\big) = \text{sign}\left(-\frac{G_x}{G_y} - \left(-\frac{F_x}{F_y}\right)\right) < 0.$$

Hence, E_3 is an unstable saddle in this subcase. The stability of equilibrium E_3 does not change, therefore, $P = 0.026391$ is not a bifurcation value. ∎

Acknowledgment. The authors are very grateful for the many valuable suggestions from Professor Eric Kostelich.

REFERENCES

[1] T. Andersen, J. J. Elser, and D. O. Hessen, *Stoichiometry and population dynamics*, Ecol. Lett., 7 (2004), pp. 884–900.

[2] M. R. Droop, *Vitamin B12 and marine ecology,* IV: *The kinetics of uptake, growth and inhibition in* Monochrysis lutheri, J. Mar. Biol. Assoc., 48 (1968), pp. 689–733.

[3] J. Elser, I. Loladze, A. Peace, and Y. Kuang, *Lotka re-loaded: Modeling trophic interactions under stoichiometric constraints*, Ecol. Model., 245 (2012), pp. 3–11.

[4] J. J. Elser, J. D. Nagy, and Y. Kuang, *Biological stoichiometry: An ecological perspective on tumor dynamics*, BioScience, 53 (2003), pp. 1112–1120.

[5] J. J. Elser, J. Watts, J. Schampell, and J. Farmer, *Early Cambrian food webs on a trophic knife-edge? A hypothesis and preliminary data from a modern stromatolite-based ecosystem*, Ecol. Lett., 9 (2006), pp. 295–303.

[6] R. A. Everett, J. D. Nagy, and Y. Kuang, *Dynamics of a data based ovarian cancer growth and treatment model with time delay*, J. Dynam. Differential Equations, 28 (2016), pp. 1393–1414, doi:10.1007/s10884-015-9498-y.

[7] R. A. Everett, A. Packer, and Y. Kuang, *Can Mathematical models predict the outcomes of prostate cancer patients undergoing intermittent androgen deprivation therapy?*, Biophys. Rev. Lett., 9 (2014), pp. 173–191.
[8] R. A. Everett, Y. Zhao, K. B. Flores, and Y. Kuang, *Data and implication based comparison of two chronic myeloid leukemia models*, Math. Biosci. Eng., 10 (2013), pp. 1501–1518.
[9] J. Grover, *Stoichiometry, herbivory and competition for nutrients: Simple models based on planktonic ecosystems*, J. Theoret. Biol., 214 (2002), pp. 599–618.
[10] J. Grover, *Predation, competition, and nutrient recycling: A stoichiometric approach with multiple nutrients*, J. Theoret. Biol., 229 (2004), pp. 31–43.
[11] S. Hall, *Stoichiometrically explicit food webs: Feedbacks between resource supply, elemental constraints, and species diversity*, Annu. Rev. Ecol. Evol. Syst., 40 (2009), pp. 503–528.
[12] E. J. Kostelich, Y. Kuang, J. M. McDaniel, N. Z. Moore, N. L. Martirosyan, and M. C. Preul, *Accurate state estimation from uncertain data and models: An application of data assimilation to mathematical models of human brain tumors*, Biol. Direct, 6 (2011), 64, doi:10.1186/1745-6150-6-64.
[13] Y. Kuang, J. D. Nagy, and S. E. Eikenberry, *Introduction to Mathematical Oncology*, CRC Press, London, 2016.
[14] Y. Kuang, J. D. Nagy, and J. J. Elser, *Biological stoichiometry of tumor dynamics: Mathematical models and analysis*, Discrete Contin. Dyn. Syst. B., 4 (2004), pp. 221–240.
[15] X. Li and H. Wang, *A stoichiometerically derived algal growth model and its global analysis*, Math. Biosci. Eng., 7 (2010), pp. 825–836.
[16] X. Li, H. Wang, and Y. Kuang, *Global analysis of a stoichiometric producer-grazer model with Holling type functional responses*, J. Math. Biol., 63 (2011), pp. 901–932.
[17] J. Liebig, *The Natural Laws of Husbandry*, Walton Maberly, London, 1863.
[18] I. Loladze, *Rising atmospheric CO2 and human nutrition: Toward globally imbalanced plant stoichiometry?*, Trends Ecol. Evol., 17 (2002), pp. 457–461.
[19] I. Loladze, Y. Kuang, and J. J. Elser, *Stoichiometry in producer-grazer systems: Linking energy flow with element cycling*, Bull. Math. Biol., 62 (2000), pp. 1137–1162.
[20] I. Loladze, Y. Kuang, J. J. Elser, and W. F. Fagan, *Competition and stoichiometry: Coexistence of two predators on one prey*, Theoret. Popul. Biol., 65 (2004), pp. 1–15.
[21] A. Lotka, *Elements of Physical Biology*, Williams & Wilkins, Baltimore, MD, 1925.
[22] J. McDaniel, E. Kostelich, Y. Kuang, J. Nagy, M. Preul, N. Z. Moore, and N. Matirosyan, *Data assimilation in brain tumor models*, in Mathematical Methods and Models in Biomedicine, U. Ledzewicz, H. Schattler, A. Friedman, and E. Kashdan eds., New York, Springer, 2012, pp. 227–254.
[23] C. Miller, Y. Kuang, W. Fagan, and J. J. Elser, *Modeling and analysis of stoichiometric two-patch consumer–resource systems*, Math. Biosci., 189 (2004), pp. 153–184.
[24] J. D. Morken, A. Packer, R. A. Everett, J. D. Nagy, and Y. Kuang, *Mechanisms of resistance to intermittent androgen deprivation therapy identified in prostate cancer patients by novel computational method*, Cancer Res., 74 (2014), pp. 2673–2683.
[25] A. Packer, Y. Li, T. Andersen, Q. Hu, Y. Kuang, and M. Sommerfeld, *Growth and neutral lipid synthesis in green microalgae: A mathematical model*, Bioresour. Technol., 102 (2011), pp. 111–117.
[26] A. Peace, *Effects of light, nutrients, and food chain length on trophic efficiencies in simple stoichiometric aquatic food chain models*, Ecol. Model., 312 (2015), pp. 125–135.
[27] A. Peace, H. Wang, and Y. Kuang, *Dynamics of a producer-grazer model incorporating the effects of excess food nutrient content on grazer's growth*, Bull. Math. Biol., 76 (2014), pp. 2175–2197.
[28] A. Peace, Y. Zhao, I. Loladze, J. Elser, and Y. Kuang, *A stoichiometric producer-grazer model incorporating the effects of excess food-nutrient content on consumer dynamics*, Math. Biosci., 244 (2013), pp. 107–115.
[29] T. Portz, Y. Kuang, and J. D. Nagy, *A clinical data validated mathematical model of prostate cancer growth under intermittent androgen suppression therapy*, AIP Adv., 2 (2012), 011002, doi:10.1063/1.3697848
[30] H. Stech, B. Peckham, and J. Pastor, *Enrichment in a general class of stoichiometric producer-consumer population growth models*, Theoret. Popul. Biol., 81 (2012), pp. 210–222.
[31] R. Sterner and J. J. Elser, *Ecological Stoichiometry*, Princeton University Press, Princeton, NJ, 2002.

[32] V. Volterra, *Fluctuations in the abundance of a species considered mathematically*, Nature, 118 (1926), pp. 558–600.
[33] H. Wang, Y. Kuang, and I. Loladze, *Dynamics of a mechanistically derived stoichiometric producer-grazer model*, J. Biol. Dyn., 2 (2008), pp. 286–296.
[34] H. Wang, R. Sterner, and J. J. Elser, *On the "strict homeostasis" assumption in ecological stoichiometry*, Ecol. Model., 243 (2012), pp. 81–88.
[35] F. Touratier, J. Field, and C. Moloney, *A stoichiometric model relating growth substrate quality (C:N:P ratios) to N:P ratios in the products of heterotrophic release and excretion*, Ecol. Model., 139 (2001), pp. 265–291.